Physica C 324 (1999) 39–46

# Growth mode study of ultrathin HTSC YBCO films on YBaCuNbO buffer

I. Grekhov, L. Delimova *, I. Liniichuk, A. Lyublinsky, I. Veselovsky, A. Titkov, M. Dunaevsky, V. Sakharov

*Ioffe Institute, Russian Academy of Sciences, 26 Polytekhnicheskaya, St. Petersburg, 194021, Russian Federation*

Received 9 February 1999; received in revised form 7 July 1999; accepted 19 July 1999

**Abstract**

It is known that the critical temperature $T_c$ of ultrathin YBCO films is reduced to values far less than 77 K. To improve the superconducting properties of ultrathin YBCO films, we developed a new buffer layer which allowed an increase in the critical temperature of five-unit-cell-thick YBCO films to values above 77 K. Using atomic force microscopy (AFM) to study the growth modes of ultrathin YBCO films deposited on a $SrTiO_3$ substrate and on a YBaCuNbO buffer layer, we found that ultrathin YBCO films deposited on a $SrTiO_3$ substrate are formed due to 2D nucleation. The growth of ultrathin YBCO films deposited on YBaCuNbO buffer is governed by the step-flow mode. As a consequence of the different growth modes, the ultrathin films deposited on a $SrTiO_3$ substrate and a YBaCuNbO buffer layer have different surface morphologies and superconductive properties. We believe that the step-flow mode makes it possible to improve the ultrathin YBCO film structure and increase the critical temperature. 

*Keywords:* Growth mode; HTSC ultrathin film; Buffer layer

## 1. Introduction

The interest in fabricating high-quality ultrathin (less than 10 nm in thickness) superconducting (HTSC) films is due to both their fundamental HTSC properties and possible microwave and microelectronic applications. It is known [1–5] that the critical temperature $T_c$ of ultrathin $YBa_2Cu_3O_7$ (YBCO) films is reduced to values far less than the nitrogen boiling point 77 K (see Fig. 1a). There are several factors, both fundamental and technological, which are responsible for the observed lowering of $T_c$. These are the transfer of mobile charge carriers across the interface, the Kosterlitz–Thouless transition, the lattice mismatch between the substrate and the film, the presence of imperfections at the interface, and so on. To improve the superconducting properties of ultrathin YBCO films, we developed a new buffer layer [6], a dielectric material composed of superconducting YBCO grains and $YBa_2NbO_6$ (YBNO) insulator grains. To fabricate such a buffer layer, we used Nb-doped YBCO (YBaCuNbO) composed of the elements Y:Ba:Cu:Nb:O in the proportions 1:2:$(3-x)$:$x$:7 with $x > 0.3$. This allowed an increase in the critical temperature of a five-unit-cell-thick YBCO film to a value above 77 K (see Fig. 1b). The purpose of the present report is to compare the observed variation in $T_c$ (Fig. 1) with

* Corresponding author. Tel.: +7-812-247-9311; fax: +7-812-247-9123; e-mail: ladel@pop.ioffe.rssi.ru

0921-4534/99/$ - see front matter 
PII: S0921-4534(99)00423-2

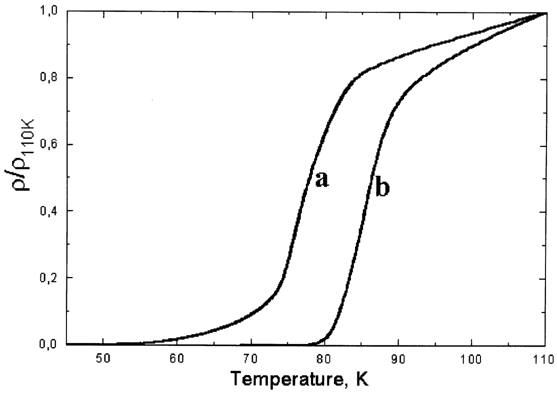


Fig. 1. Resistance versus temperature for 6 nm thick YBCO films deposited on (a) a $SrTiO_3$ substrate, and (b) a YBaCuNbO buffer layer.

the growth mode. We present the results of atomic force microscopy (AFM) studies of ultrathin YBCO films deposited on a $SrTiO_3$ substrate and on a YBaCuNbO buffer layer.

## 2. Experimental results

All the films studied were fabricated using the laser ablation technique; the details are given in Ref. [6]. The average deposition rate of about 0.03 nm/s was evaluated from optical ellipsometry data, profilometer measurements, and Rutherford backscattering spectra. The ultrathin YBCO film thickness was controlled by high depth resolution Rutherford backscattering spectrometry. The energy spectra of $He^+$ ions with the initial energy of 190 keV, scattered to the angle of 120°, were measured by means of a half-spherical electrostatic analyzer having the energy resolution $\Delta E/E \approx 5 \times 10^{-3}$. Random and aligned spectra for a typical YBCO ultrathin film, together with the result of random spectrum computer simulation, are given in Fig. 2. From this simulation, we deduced the composition of the film to be Y:Ba:Cu = 0.7:2.2:3, which is close to the stoichiometric one, and the film thickness of $6.1 \times 10^{16}$ atoms/cm$^2$. Assuming the density to be

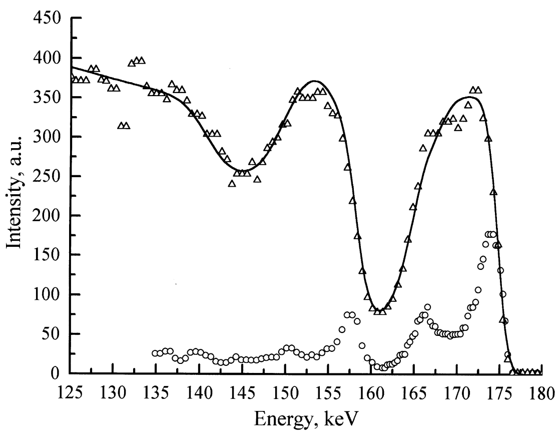


Fig. 2. Aligned (circles) and random (triangles) backscattering spectra of a typical ultrathin YBCO film. The solid curve is the result of computer simulation.

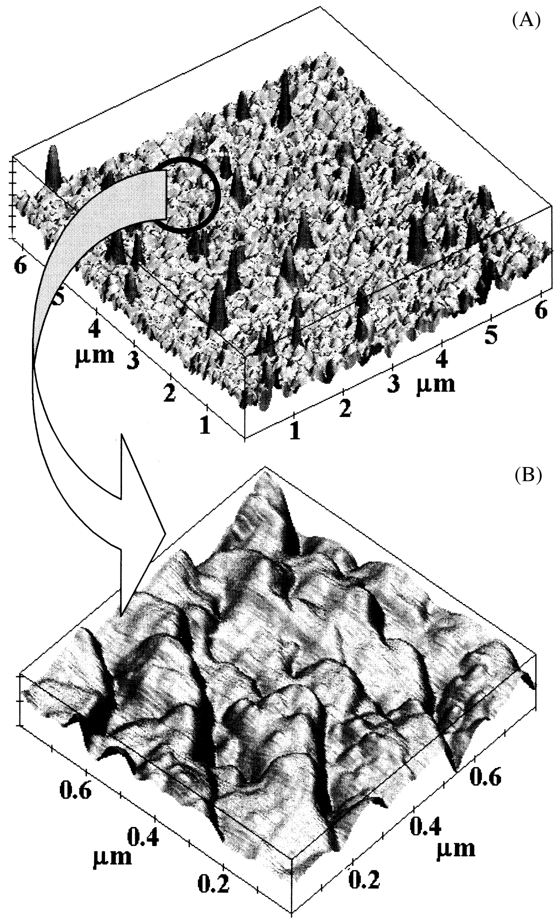


Fig. 3. AFM images of a 6 nm thick YBCO film deposited on a $SrTiO_3$ substrate: (A) the general view, (B) the blow-up region of the film among the outgrowths.

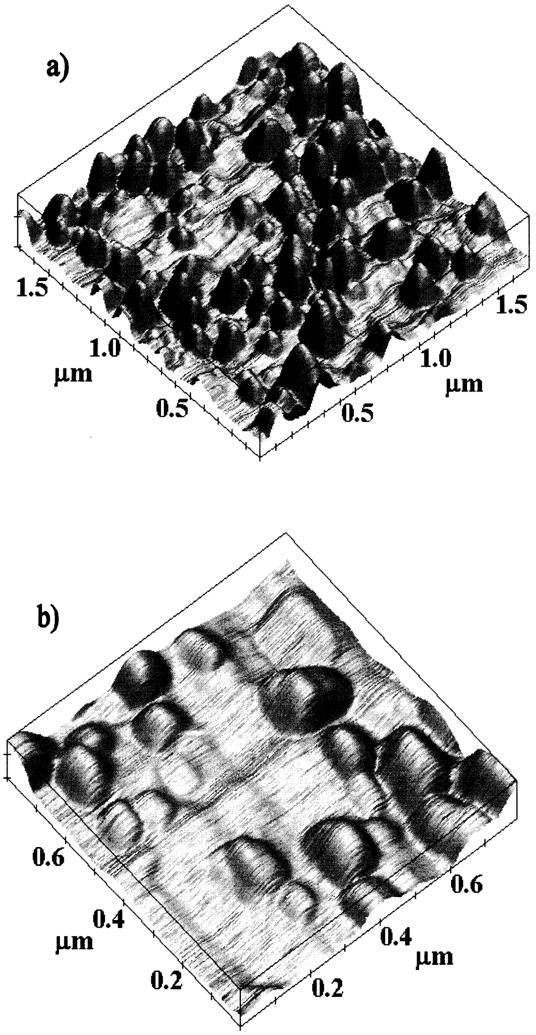


Fig. 4. AFM images of a 30 nm thick YBCO film on a $SrTiO_3$ substrate: (a) the general view, (b) the blow-up top right part of the general view.

6.35 $g/cm^3$, this thickness corresponds to 8.2 nm. The minimum relative yield, or the aligned-to-random ratio, obtained for the regions close to the low-energy edges of the surface peaks, revealed the medium value of 0.12, which is an evidence for an extremely high crystalline quality of the film. Thus, when we refer to a film as thick as 8.2 nm, we mean that the amount of deposited YBCO corresponds to a uniform coverage of 8.2 nm.

The sample surface structure was investigated by AFM, using a P4-SPM-MOT device. Surface images were obtained under ambient conditions in the constant-force mode. We used a $Si_3N_4$ tip of 30 nm radius, which provided a reliable observation of even monatomic steps. All of the films were deposited on $SrTiO_3$ (100) substrates, with the (100) axis misoriented by less than 10′, and the substrate surface roughness was about 1–2 nm high.

An AFM image of a 6 nm thick YBCO film deposited on a $SrTiO_3$ substrate is illustrated in Fig. 3a. One can see that the film is not entirely smooth but contains islands or outgrowths of about 10–40 nm high and 130–400 nm in diameter. The outgrowths occupy about 4% of the film surface, with the average distance between them of about 1 µm. The film is seen to be rather smooth among the outgrowths, which is illustrated by a magnified re-

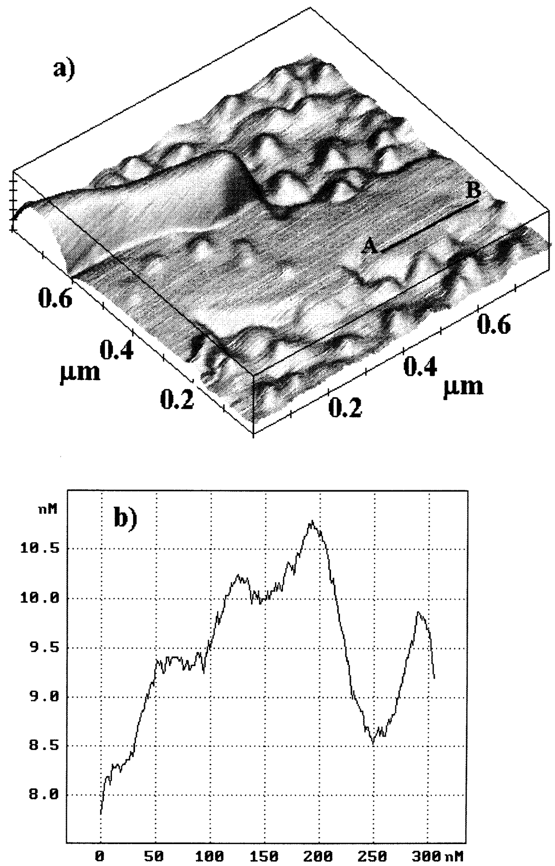


Fig. 5. An AFM image of a 30 nm thick YBaCuNbO buffer layer on a $SrTiO_3$ substrate: (a) some specific features in the buffer surface morphology, (b) the line-scan profile along the AB line.

gion in Fig. 3b. Note that the film grains are asymmetric and elongated. The largest grains are 200 nm long, and the largest peak-to-valley surface is 4 nm high. There are 2D nuclei well-defined on the grain surface. These features suggest 2D nucleation and a layer-by-layer (Frank–van der Merwe) growth mode. In contrast to this, the image of a 30 nm thick YBCO film reveals a 3D island formation, as is seen in Fig. 4. Against the relatively flat background, there are islands resembling a stretched barrel, with heights of about 5–40 nm and lateral dimensions within the range 100–150 nm. This is a layer-by-layer growth followed by island growth (the Stranski–Krastanov mode). These observations of YBCO films deposited on $SrTiO_3$ substrates are in good agreement with the results of Ref. [7].

The buffer layer we used is a dielectric; its resistivity at room temperature as high as $6.1 \times 10^3$ $\Omega$ cm corresponds to a resistance value of about $10^8$ $\Omega$ for a 30 nm thick buffer layer. The buffer layer represents a mixture of two phases: superconducting YBCO and insulating YBNO, approximately in equal proportions [6]. The X-ray diffraction patterns of a 100 nm thick YBaCuNbO buffer layer indicate an orthorhombic structure of $c$-oriented YBCO grains and a cubic structure of YBNO grains with the [100] direction normal to the film surface and a lattice constant $a = 0.84$ nm. The crystal lattice parameter $c$

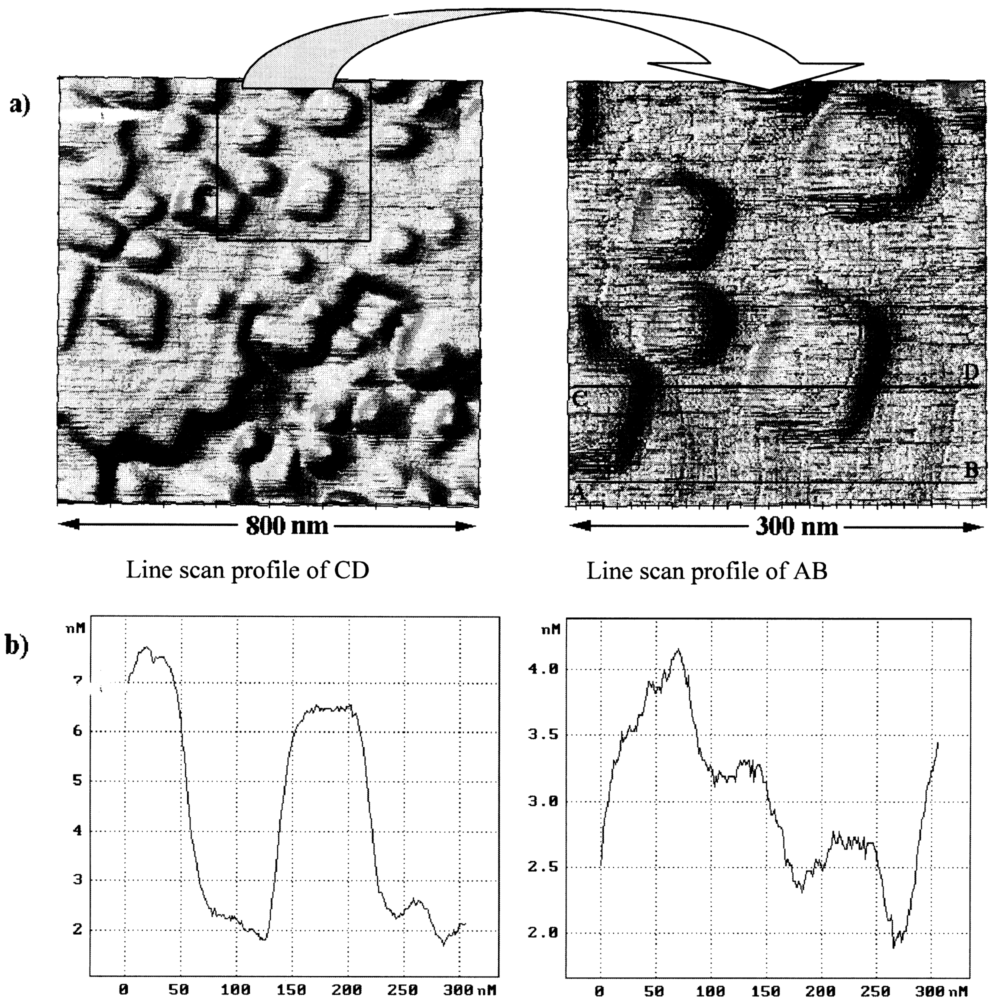


Fig. 6. Surface morphology of the YBNO insulator phase: (a) AFM images of the plateau, (b) the line-scan profiles along the plateau.

of YBCO grains in the buffer layer increased to $1.174 \pm 0.004$ nm, which resulted either from the crystal tension or the oxygen loss in the YBCO grains. The YBCO and YBNO grain size obtained from X-ray diffraction data is as large as 30 nm, which allows us to suggest that a 100 nm thick YBCO film is free from crystal tension and that the large value of the parameter $c$ indicates a lower oxygen content. This result correlates with Raman scattering spectrometric data, which also supports a reduction in the oxygen content in the YBCO phase of an YBaCuNbO buffer layer [6]. According to Ref. [8], the value $c = 1.174$ nm corresponds to oxygen deficit of about 0.47. It is very close to the orthorhombic–tetragonal transition point, and the critical temperature for this YBCO composition is lower than $T_c = 50$ K. In addition, X-ray diffraction shows an asymmetric line for the YBCO phase, suggesting a nonuniform oxygen distribution throughout the YBCO phase. Thus, we can assume that the YBCO phase in the buffer layer is superconducting, with the critical temperature far lower than 77 K.

Fig. 5 shows an AFM image of a 30 nm thick YBaCuNbO buffer layer deposited on a $SrTiO_3$ substrate. The surface morphology is seen to have some specific features: the YBCO phase produced in the island growth mode (the $c$-axis is normal to the substrate plane), some amount of YBCO looking like a crest (we believe this to be the YBCO phase with the $c$-axis oriented in the substrate plane), and a very smooth plateau of about 12 nm high. The plateau roughness is illustrated by the line-scan profile along the AB line, with three steps of about 0.8 nm high at a distance of 50 nm. The value of the step height is close to the lattice constant of the YBNO insulator phase, $c = 0.84$ nm; thus, we can assume that this plateau is an YBNO insulator phase and the steps indicate the step-flow mode [9]. Fig. 6 shows a more detailed image of this plateau. There are 2D rectangular nuclei with a very flat top on the plateau surface. Indeed, the top roughness is 1–2 nm high over a distance of about 60 nm (see line-scan profile along the CD line). The outlines of the plateau reproduce the contours of these rectangular nuclei indicating that the plateau has resulted from the coalescence of 2D nuclei. The line-scan profile along the AB line on the plateau shows growth steps of 0.8 nm high. The presence of 2D nuclei and the growth steps on the same YBNO plateau indicate a competition between 2D nucleation and localized step propagation (the birth and spread mode) [9]. It should be noted that both YBCO islands and the insulator YBNO plateau coexist side by side. At the phase boundary, one can see a few YBCO islands which were formed on the insulator plateau. We believe that these YBCO nuclei are of principal importance since they may serve as nucleation sites for a new YBCO molecular layer during the deposition.

Let us now consider the formation of an YBCO film on a buffer layer. We have analyzed five YBCO samples grown on YBaCuNbO. Fig. 7 shows a typical AFM image of a 4 nm thick YBCO film on an

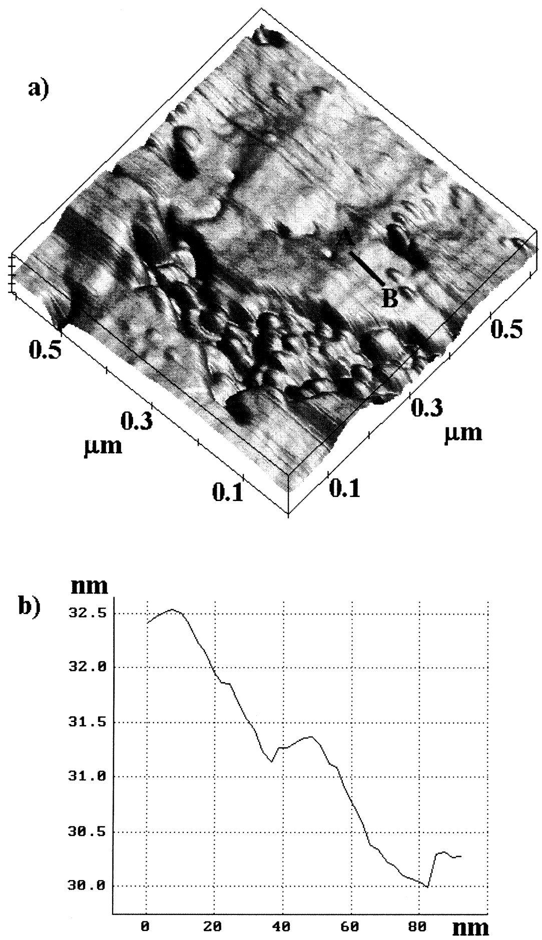


Fig. 7. An AFM image of a 4 nm thick YBCO film on an YBaCuNbO buffer layer: (a) a 3D image, (b) the line-scan profile along the AB line.

YBaCuNbO buffer. Two regions can be easily distinguished in the film surface morphology: that of islands and of a plateau. The island region looks like the buffer YBCO phase. There are growth steps of about 1.2 nm high on the plateau. This step value is close to the YBCO lattice constant in the *c*-axis, suggesting that the plateau has been formed from the YBCO phase. Fig. 8 shows AFM images of a 6 nm thick YBCO film on an YBaCuNbO buffer layer. The general view shows that the plateau region occupies most of the film surface, and contains voids where the film is not formed. There are growth steps of about 1.2 nm high on the plateau, and their size is close to the YBCO lattice constant. This is an evidence that the plateau has resulted from the YBCO phase. Fig. 9 illustrates AFM images of a 12 nm thick YBCO film on an YBaCuNbO buffer layer. The general view of the film shows that most of the film is occupied by a plateau region. One can see that in the magnified plateau image the voids have grown smaller in size, compared to the 6 nm thick YBCO film. There is a number of growth steps as high as 1.2 nm, pointing to the fact that the plateau represents the YBCO phase.

We can suggest from the results presented in Figs. 7–9 the following mechanism of the ultrathin YBCO film growth on YBaCuNbO. The buffer film is formed by the YBCO islands and the YBNO plateau.

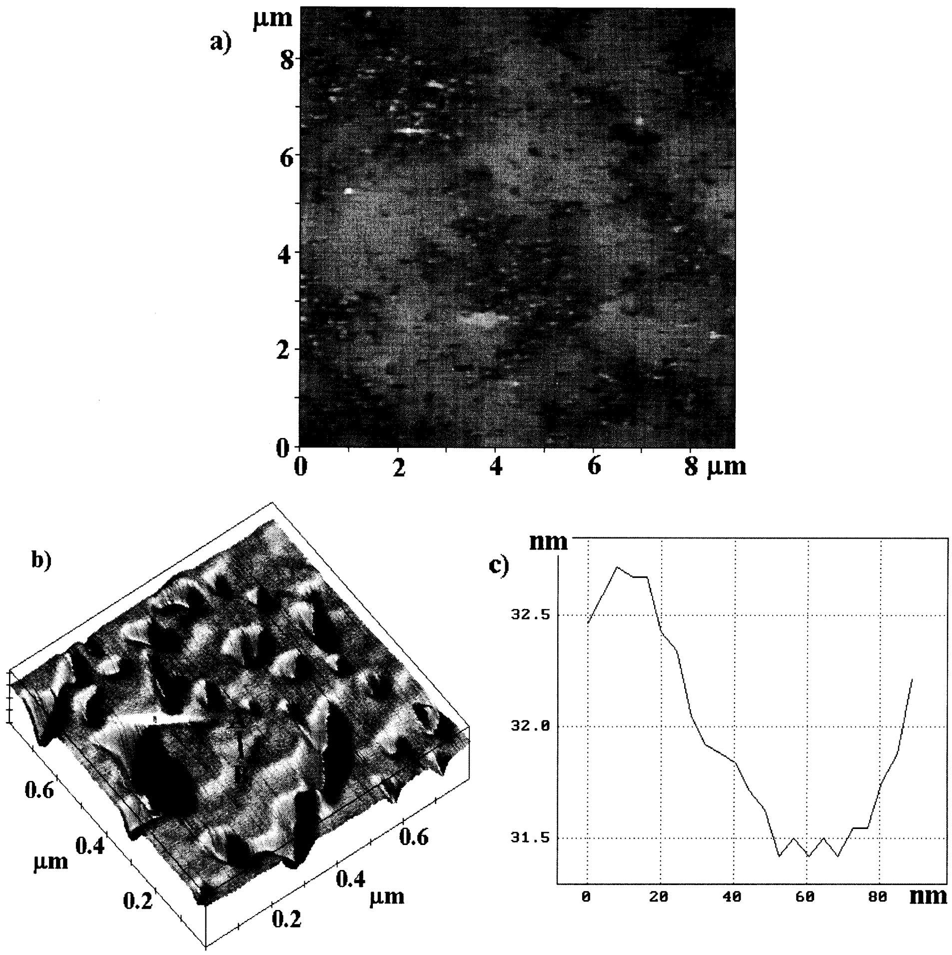


Fig. 8. AFM images of a 6 nm thick YBCO film on YBaCuNbO buffer: (a) the general view, (b) the magnified image of the plateau, (c) the line-scan profile along the AB line.

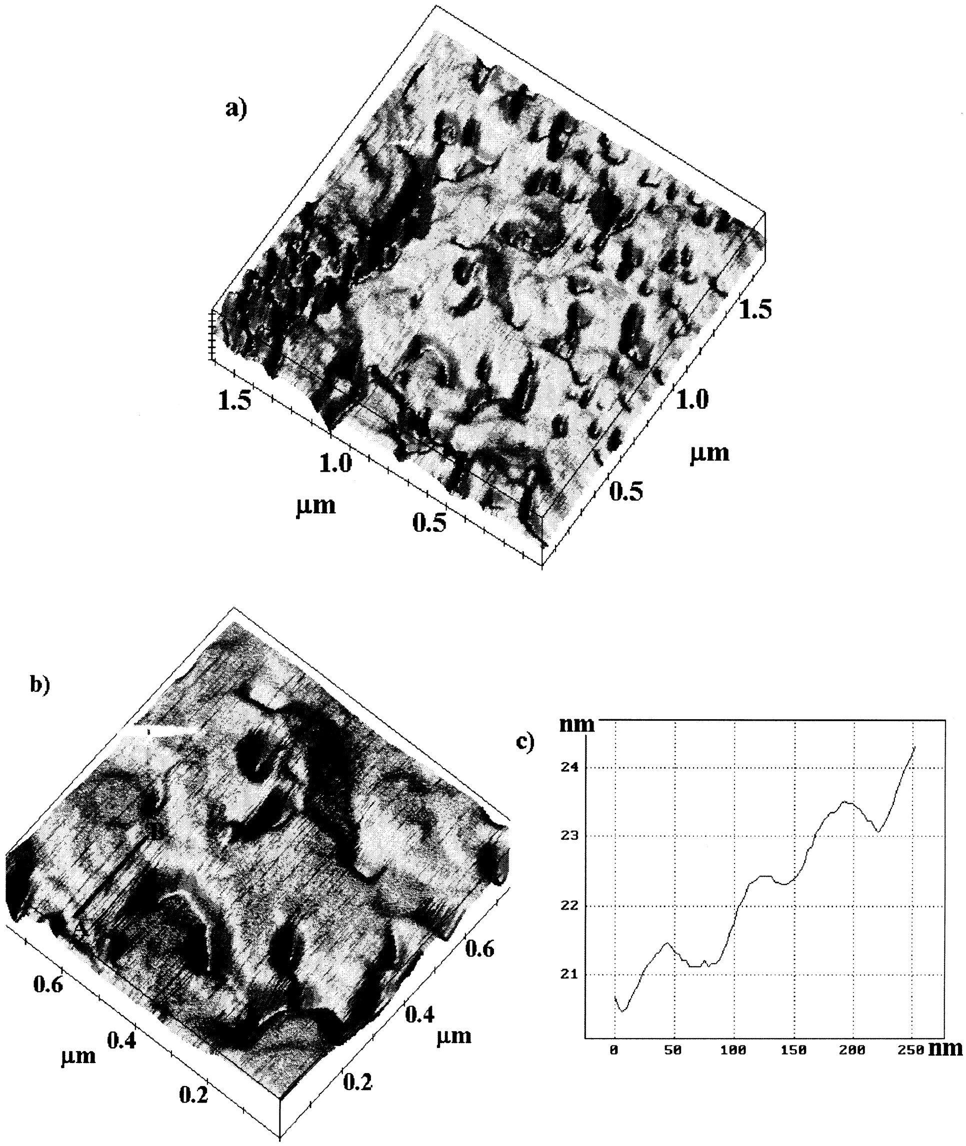


Fig. 9. AFM images of a 12 nm thick YBCO film on YBaCuNbO buffer: (a) the general view, (b) the magnified image of the plateau, (c) the line-scan profile along the AB line.

The sputtered YBCO material is deposited on the buffer and covers both the YBCO islands and the YBNO plateau, so that the barrel-shaped YBCO nuclei can be visible on the surface. The YBCO growth in the *a–b* plane is more favorable on the YBNO plateau than on the YBCO islands. The YBNO plateau is very flat with a few YBCO nuclei on its surface. They serve as the nucleation sites for a new YBCO molecular layer which spreads over the plateau via the localized step propagation. The YBCO islands of the buffer layer cannot provide favorable conditions for film spread in the *a–b* plane, which may result in the formation of voids in the YBCO film. As the amount of the deposited YBCO increases, the growing film propagates, the voids grow smaller, and the film looks like foam covering the islands.

It should be mentioned, however, that a considerable mismatch between the lattice constants of YBCO and YBNO is of importance. The misfit between substrate and HTSC layer is known to have a dramatic effect on the surface nucleation and growth modes: the misfit reduces the step-flow regime (layer-by-layer growth) and enhances the 2D nucleation (island formation) [9]. The strain produced by the misfit may be partially or completely relaxed by the formation of misfit dislocations, microcracks, etc. It is surprising that a film growing on the YBNO plateau manifests a high superconductive property ($T_c$) in spite of the considerable misfit between the YBCO and YBNO lattices. We believe this is due to the fact that a new film nucleates and starts growing from the YBCO nuclei on the YBNO plateau with no mismatch in the lattice constants. The film growth occurs via the localized step propagation. It seems likely that the lattice mismatch between the ultrathin YBCO film and the YBNO plateau for the film nucleation described and for reasonably short inter-step distances (30–50 nm) is of no importance. It will be a subject of further investigation.

## 3. Conclusions

We have used AFM to study the growth modes of ultrathin YBCO films deposited on a $SrTiO_3$ substrate and on a YBaCuNbO buffer layer. The investigation has shown that ultrathin YBCO films on $SrTiO_3$ substrates are formed due to 2D nucleation, as was observed in Ref. [7]. The growth mechanism of an ultrathin YBCO film deposited on a YBaCuNbO buffer layer is governed by the step-flow mode. As a consequence of the different growth modes, an ultrathin film on a $SrTiO_3$ substrate and YBaCuNbO buffer have different surface morphologies and superconductive properties ($T_c$). We believe that the step-flow mode makes it possible to improve the ultrathin YBCO film structure and increase the critical temperature.

## Acknowledgements

This research was supported by the Russian Ministry of Sciences grant no. 96068.

## References

[1] X.X. Xi, C. Doughty, A. Walkenhorst, C. Kwon, Q. Li, T. Venkatesan, Phys. Rev. Lett. 68 (1992) 1240–1243.
[2] J. Mannhart, D.G. Schlom, J.G. Bednorz, K.A. Muller, Phys. Rev. Lett. 136 (1992) 555.
[3] J. Gao, W.H. Wong, J. Xhie, Appl. Phys. Lett. 67 (1993) 2232–2234.
[4] M.Z. Cieplak, S. Guha, S. Vadlamannati, T. Giebultwicz, P. Lindenfeld, Phys. Rev. B 50 (1994) 12876–12886.
[5] Y.N. Drozdov, Y.N. Nozdrin, A.E. Parafin, S.A. Pavlov, V.V. Talanov, A.V. Varganov, E.A. Vopilkin, IEEE Trans. Appl. Supercond. 7 (1997) 1491–1497.
[6] I. Grekhov, M. Baydakova, V. Borevich, V. Davydov, L. Delimova, I. Liniichuk, A. Lyublinsky, Physica C 276 (1997) 18–24.
[7] X.Y. Zheng, D.H. Lowndes, S. Zhu, J.D. Budai, R.J. Warmack, Phys. Rev. B 45 (1992) 7584–7587.
[8] Y. Kubo, T. Yoshitake, J. Tabuchi et al., Jpn. J. Appl. Phys. 26 (1987) L768–L770, Part 2.
[9] H.J. Scheel, in: T. Fujita, Y. Shiohara (Eds.), Advances in Superconductivity, Vol. VI, 6th Intl. Symp. on Superconductivity, Hiroshima, Oct. 1993, Springer, Tokyo, 1994, p. 29.